

Article

Magnetic Survey for Iron-Oxide-Copper-Gold (IOCG) and Alkali Calcic Alteration Signatures in Gadarwara, M.P, India: Implications on Copper Metallogeny

P.V. Sunder Raju * and K. Satish Kumar

Council of Scientific and Industrial Research-National Geophysical Research Institute, Uppal Road, Hyderabad, Telangana 500007, India; satishmarine_777@yahoo.co.in

* Correspondence: pvsraju@ngri.res.in

Received: 24 April 2020; Accepted: 6 July 2020; Published: 29 July 2020



Abstract: A government airborne geophysical survey flown in the late 1970s detected a large Magnetic anomaly at Gadarwara, Madhya Pradesh, in north-central India. Deep drilling indicates that the oval-shaped Magnetic anomaly is caused by underlying Magnetite-bearing banded iron formation belonging to the Mahakoshal Formation of Archean to Early Proterozoic age. The anomaly is hosted in a tectonic rift zone (Narmada-Son Lineament). After drilling alluvium up to 312 m thick, rocks intersected to depths of 612 m provided core samples for research. Broadly speaking, the samples contain banded hematite jaspilite (BHJ) and banded Magnetite (BM) iron formation with pervasive carbonate alterations. Three vertical diamond drill holes were drilled along a 1.4 km long N-S transect across the center of the geophysical anomaly. DDH-1, near the northern edge of the anomaly, went through 309 m of alluvium before intersecting bedrock and then cored 303 m of bedrock for a total depth of 612 m. Copper mineralization with appreciable amounts of cobalt, zinc, molybdenum, silver, rare earth elements, uranium and other elements was intersected. The litho-units are highly oxidised and intensely brecciated with hydrothermal overprinting of Na-K metasomatism alteration mineralogy. The second borehole, DDH-2 failed as the core drilling bit stuck in the alluvium and further drilling was abandoned, whereas the third borehole DDH-3 did not intersect a Magnetite-hematite association and cored only siltstone. Two-dimensional model studies suggest that the signature of high Magnetic anomaly is at a depth of 0.4 km from the surface, with a width of 3.5 km, dipping at 45° in a northerly direction. The causative body has a Magnetic susceptibility of 0.0052 C.G.S. units, suggestive of a hematite with quartz veinlets lithology. Based on predictive Magnetic exploration models for Iron-Oxide-Copper-Gold (IOCG), such deposits can be inferred from geological observations combined with petrophysical data and forward modelling of the observed Magnetic signatures. This paper reports a prospective IOCG-like mineralization style hosted in a rift (Narmada-Son) type of tectonic environment.

Keywords: Gadarwara; central India; mineralization; IOCG; Narmada-Son-Lineament; Magnetic anomaly

1. Introduction

Magnetic surveys are rapid and provide clues from prospect to province. Magnetic anomalies can also provide direct signatures of certain types of ore deposit or mineralization. IOCG provinces extent across the globe and range in geological timescales from Archean to Cenozoic and include the modern examples such as Iron-Oxide Copper Gold (IOCG), the Kiruna type IO ± A (Iron Oxide Apatite) [1,2]: Examples include the Gawler craton [3,4], Olympic Dam, Clonclurry, Tennant Creek in Australia [5–8], Kiruna in Sweden and Carajas, in Brazil [9,10], and the lesser understood Wernecke [11],

Great Bear Magmatic zone [12] in the Canadian shield [12], Khetri [6,13] and Singhbhum [14] deposits in India. The majority of these key deposits and districts are Paleo- or Mesoproterozoic in age, they have vast extents $<35 \text{ km} \times 1.5 \text{ km}$, occur at depths of 3–10 km in an active Magmatic setting [15].

They can vary in alteration facies (Na-Ca-Fe-K-Mg) and chemical footprints range from cm-m-km scale [16]. The salient features of IOCG include the following [6]: (1) The occurrence of copper (Cu) with or without gold (Au); (2) Hydrothermal vein, breccia or replacement ore styles characteristically in specific structural sites; (3) Abundant Magnetite or hematite; (4) Iron oxides which have low Ti contents compared to those in most igneous rocks and bulk crust, in particular nelsonites and igneous Fe-Ti deposits; (5) Absence of clear spatial association with igneous intrusions.; (6) Strong structural and stratigraphic control; (7) abundant hydrothermal-structural breccia zone. The geological architecture and evolution of India show it to have rocks from Archean to Phanerozoic ages, and suitable geological settings [6] as potential hosts for IOCG/Kiruna-type deposits. However, in India reports on IOCG are documented from the Bhukia IOCG-IOA deposit of Aravalli-Delhi Fold Belt, Rajasthan, western India [14,17], Thanewasna, Western Bastar Craton [18], Singhbhum Craton [14], and Machanur, Eastern Dharwar Craton [19] (Figure 1). The Council of Scientific and Industrial Research- National Geophysical Research Institute (CSIR-NGRI), India carried out an airborne geophysical survey flown in the late 1970s and detected a sizeable Magnetic anomaly at Gadarwara, Madhya Pradesh, in north-central India [20] with only scanty follow-up studies. For the first time, we provide the geophysical signatures using an integrated investigation with new insights on geophysical and geochemical characteristics of these rocks and offer unique constraints on the nature and significance of the IOCG mineralization at Gadarwara, Madhya Pradesh, India.

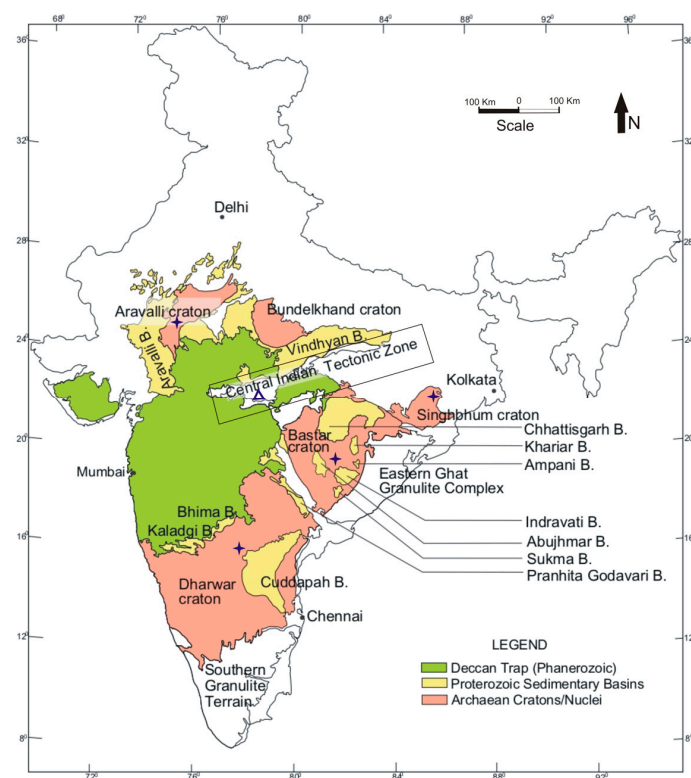


Figure 1. Simplified geological Map of India showing position of five cratonic blocks and sedimentary basins (after Mazumder et al., 2019a [21]) with reported IOCG deposits (blue stars) and study area in (triangle).

2. Regional Geology

The Son- Narmada-Tapti fault (NSF) is one of India's most prominent geomorphic features and cuts across the central part of the Indian subcontinent [1]. This east-northeast (ENE) to west-southwest (WSW) trending lineament extending in length of about ~1200 km from 72.5° E to $82.5^\circ 5'' \text{ E}$ long

and 21.5° N to 24° N latitude (Figure 2a). The NSF structural zone juxtaposes disparate and complex geological and geophysical characteristics and comprises a broad region (up to 30 km wide) of linear topographic features, contemporary seismicity, and hot springs [22]. The NSF is currently expressed as an alluvium-filled tectonic rift zone with northern and southern bounding faults. More importantly, the Son- Narmada-Tapti fault divides the Bundelkhand Craton to the north from the Dharwar Craton to the south. The Bundelkhand Craton consists of Archean amphibolitic and ultramafic slivers of greenstone belt association within a broader region of poly-metamorphosed sialic and TTG gneisses (ca. 3.5–2.7 Ga), metamorphosed volcano-sedimentary rocks, and syn- to post-tectonic granitoids (ca. 2.5–2.4 Ga), and granitoids that include a significant Paleoproterozoic component. The older rock packages are cut by at least three generations of Mafic dyke swarms, most importantly the ca. 1700 Ma dolerite dykes that are likely related to the development of rift basins of the Bijawar (or Mahakoshal Group) and Gwalior Formations. The overall tectonic trend of the Bundelkhand Craton (Figure 2b) is E to ENE flanked along its southern and northwestern Margins by the Pre-Vindhyan siliciclastic shelf sequence of the Bijawar Formation. The eastern, western and southern Margins of the BKC are covered by Vindhyan Group rocks (1400 Ma and younger), while the alluvium is covered in the northern border [23]. The stratigraphy of study area is shown in Table 1.

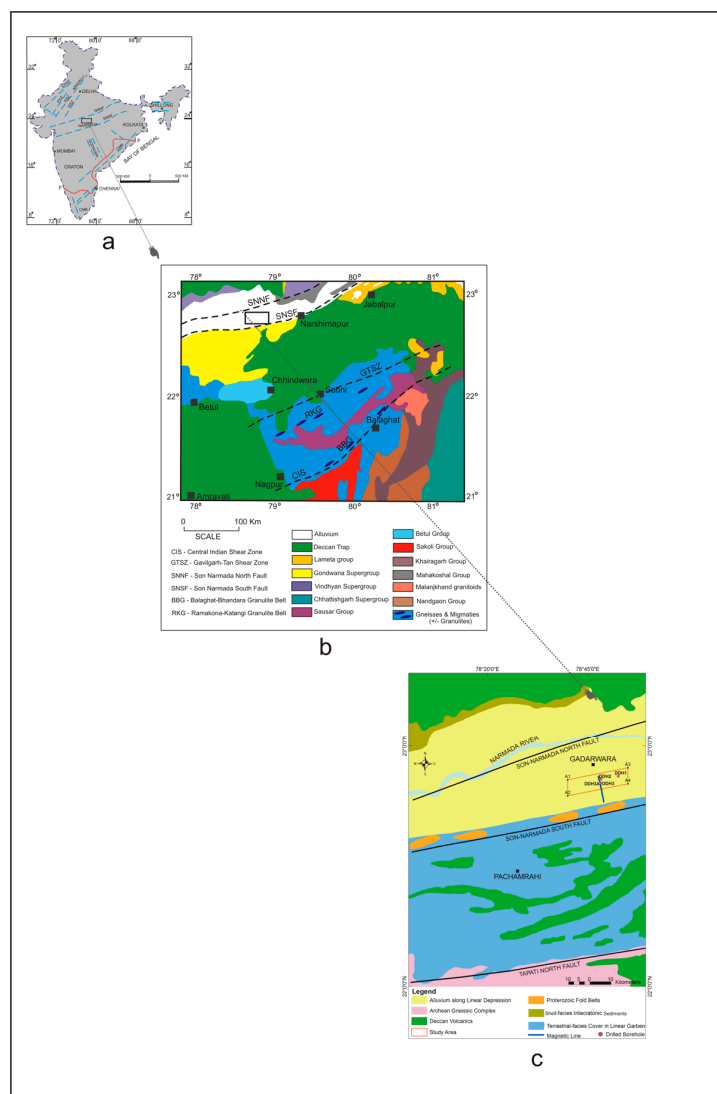
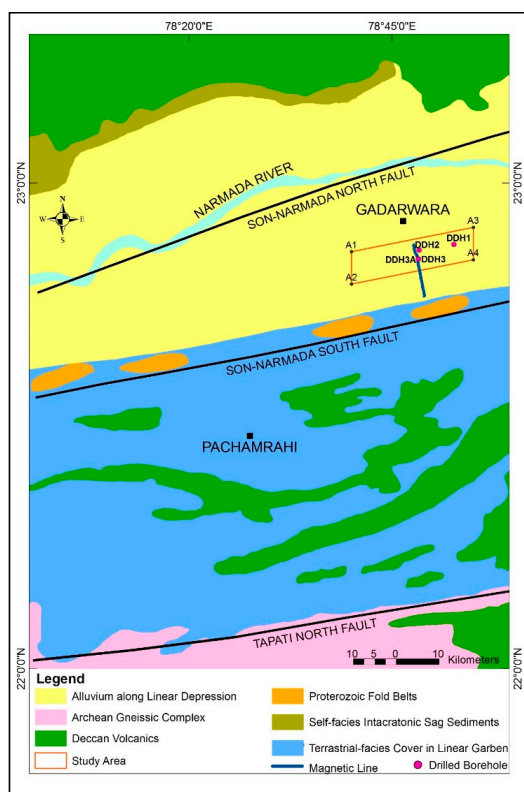


Figure 2. Cont.



(B)

Figure 2. (A): (a) Simplified Tectonic Map of India; (b) Simplified geological Map of the Central Indian Tectonic Zone in central India, showing all the supracrustal belts and tectonic lineaments (modified after Yedekar et al. 1990 [24], Acharyya and Roy 2000 [25], Chattopadhyay and Khasdeo 2011 [26]); (c) Geological Map of Study area (after Sunder Raju., 2014 [27]). (B) Geological Map of the Study area.

Table 1. The stratigraphic sequence of the Narmada-Son lineament belt.

Age		Group
Recent		Alluvium (study area)
Pleistocene		Laterite
Eocene		Trap intrusions, dolerite dykes, intertrappean beds, Deccan trap dikes, Deccan trap flows, Bagh beds, Lameta beds
		unconformity
Lower Cretaceous	Gondwana	Upper Gondwana
Upper Carboniferous		Lower Gondwanas
Lower Paleozoic	Vindhyan	Upper Vindhyan
Upper Precambrian	Super Group	Lower Vindhyan
Lower Proterozoic	Bijawar Group	Limestones, quartzites
		unconformity
Archean		Granites, gneisses, schists and phyllites

The generalise stratigraphic succession of the region (modified after Geological Survey of India publication: Mallet 1869 [28]; GSI, 1976 [29]).

The Mahakoshal Supergroup (Figure 2b) has a linear, east-north-easterly-trending zone between the two cratonic regions (Dharwar, Bundelkhand) and mostly exposed within the bounding faults of the Narmada Son Lineament [30]. The Bundelkhand craton consist of metavolcanic and metasedimentary rock sequences with significant basic/ultrabasic intrusions formed in a rift environment [30]. The older parts of the Mahakoshal Supergroup are siliciclastic and variably referred to as the Bijawar group (ca 2600–2400 Ma) [31] which at their type section in the Son Valley, lacks the deformation and associated intrusions of the Mahakoshal in the Narmada valley. The Mahakoshal Supergroup includes the Sakoli and Nandgaon bimodal volcanics with Dongargarh and Malanjkhanda K-granite island-arc type

intrusions from a Paleoproterozoic period (2.2–2.3 Ga) in the Bhandara craton. The Mahakoshal Group exposed in the Son valley was intruded by Alkali syenite and lamprophyre at 1796 Ma to 1610 Ma [32]. The Mahakoshal was deformed by folding and faulting resulting from Meso- to Neoproterozoic convergence [30] and is therefore locally and otherwise known as the Mahakoshal Deformed Zone. The Vindhyan Basin (Figure 2b) rocks unconformably overlap upon older Mahakoshal and Bijawar Supergroups and Bundelkhand cratonic rocks. The Vindhyan Group consist of quartzites of 5–6 km thick pile associated with metasedimentary rocks that are divisible into a Lower Group (Semri Series) of ~1.7 Ga [33] and Upper Group (Kaimur, Bhandar and Rewa Series) that are 1.1 to 0.7 Ga. Pyroclastic units and felsites and sedimentological changes indicate changes in basin architecture, likely due to fault reactivations [34]. Vindhyan Group rocks are flat-lying and have not been intruded by granitoids. The northern limit of the Central Indian Tectonic Zone (CITZ) is defined by the ENE-WSW trending Son Narmada North Fault (SNNF) and is traceable from Markundi in Uttar Pradesh in the east to Hosangabad in Madhya Pradesh in the west [25]. Geologically, the lineament bounds are represented by two faults, and the Mahakoshal rocks are dominant in between these two faults, Son Narmada South Fault (SNSF) and Son Narmada North Fault (SNNF). (Figure 2c) [35] Further east, the rift faults and associated folds crop out with their subsidiary structures. Locally along the rift in the east, there are gold and base metal deposits of various types which are economically viable [30]. The BIFs found are classified as of Algoma type [30].

3. Methodology

3.1. Magnetic Survey

A ground Magnetic traverse of 15-line km was carried out in the study area by a private party. The approximate bearing of the traverse was 170–350°. The survey utilized two GEM Systems GSM-19W Magnetometers, equipped with in-built GPS, and a Geometrics G856 base station Magnetometer, recording the diurnal Magnetic variation at 20 s. intervals. The study area is demarcated in Figure 3 with the Magnetic traverse and drill hole locations.

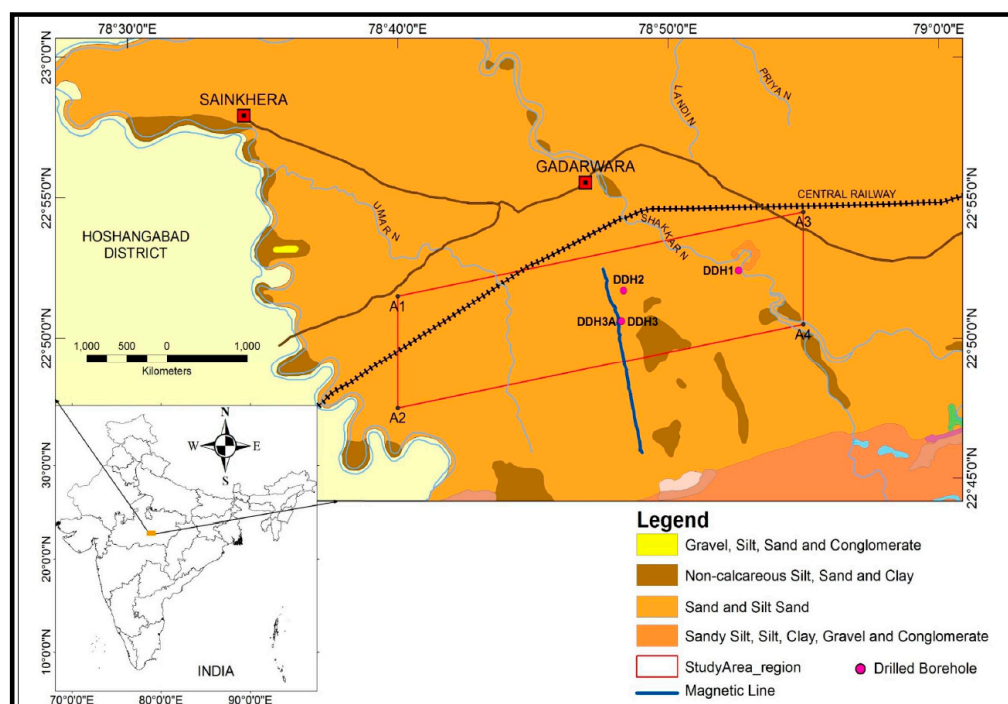


Figure 3. Study area boundaries.

3.2. The Gadarwara Magnetic Anomaly

In 1979, the CSIR-NGRI (-National Geophysical Research Institute, Hyderabad, India) carried out regional aeromagnetic surveys in three blocks along the Narmada Son Lineament for the Geological Survey of India. [36] The Magnetic data collected at a nominal line spacing of 2000 m at an altitude of 1000 m (~3200 feet). This area is mostly covered by thick alluvium and outcrops are sparse with a few exposures of the Mahakoshal Supergroup (Figure 2b). The aeromagnetic survey picked up a glaring anomaly in the central block located towards the south of Gadarwara town (22.552° N, 78.472° E) [31,37]. The magnitude of the anomaly is about a 600 nT, above background values and covers an area of approximately 40 km². This Magnetic anomaly is widespread and trends to the east-northeast, and is about 1800 m wide and 20 km long. A subsequent ground Magnetic survey better constrained the anomaly to about 1200 nT amplitude [31]. The concealed anomaly is caused by Magnetite bearing “banded Iron Formations” or BIFs. BIFs assemblages are commonly associated with IOCG deposits around the globe [6]. The dominant meta-sedimentary rocks consist of cherty BIF (CBIF) with ribbon-like jasperoids, alternating bands of crypto-crystalline to microcrystalline chert and anhedral hematite with little or no clastic admixture. The thickness of hematite layers varies (1–2 mm) and hosts sericite and chlorite-ripidolite commonly. The dominance of hematite consists of specularite with replacement of silicates and Magnetite. The common gangue mineral phases include quartz, Ca(Mg-Fe) carbonates, chlorite, sericite, and apatite. Hematite rocks contain higher sulphidic mineral contents than the Magnetite rocks. REE and U enrichments occur as discrete mineral phases. Accessory zircon and apatite occur as acicular clusters. Magnetite is prominent in all the samples, and in association with hematite. Magnetite grain shapes vary from rounded, sub-rounded, euhedral, amoeboid and mesh-like with Magnetite ex-solution appear like lamellae. Magnetite-dominated assemblages contain apatite as clusters and acicular needles. Sulphides are minor with pyrite >> chalcopyrite. Varying morphologies of zircon, monazite, and xenotime are observed in SEM studies. They are typically of ~25–50 µm in size, but difficult to further quantify because of small size and altered character.

The Main sulphides mineral assemblage consists of chalcopyrite and pyrite. In particular pyrite, are round to sub-round grains and occur in interstitial spaces within fine-grained Magnetite. The sulphidic BIFs contain calcite, siderite or ferroan dolomite. Minor hercynitic spinels also occur. The essential Fe-bearing minerals in carbonate are siderite and ankerite, with lesser ferroan dolomite, calcite and Magnesium siderite.

4. Results

4.1. Drilling Results

In 2007, Adi Gold Mining Pty. Ltd. (New Delhi, India) initiated an exploration program to drill a 1.4 km fence of three vertical diamond drill holes from north to south across the center of the geophysical anomaly. DDH-1 was drilled (Figure 4 and Table 1) from near the northern edge of the anomaly, went through 309 m of alluvium coring 303 m of bedrock for a total depth of 612 m. The litho-units encountered in the drill core (Figure 4) include felsic tuff, metasedimentary rocks dominated by banded chert, and various BIF facies, such as cherty BIF, hematite BIF, Magnetite BIF and carbonate BIF. The samples contained carbonate either as a component of the rock Matrix, within coarse-grained, quartz-rich segregations parallel to the metamorphic foliation, or in cross-cutting veins. Rock samples that were taken from drill cores had coatings of travertine, iron/jaspilite and iron oxides. The sample locations and lithology are listed in Table 2. Furthermore, the XRD results suggest and confirm the presence of sheet silicates (i.e., kaolinite, montmorillonite, dickite, mica, chlorite), iron oxides, quartz, and carbonate, etc. The DDH 1 core was strongly weathered to alteration products with hematite and goethite, and the iron oxides, Making explicit recognition of banded hematized Magnetite, red jasper and white chert beds, difficult. The beds are tightly folded, and veinlets of quartz are not uncommon with pseudomorphs and cubic cavities left by oxidized pyrite. DDH-2 advanced through 288.8 m of alluvium before being abandoned. DDH 3, located near the southern edge of the anomaly,

went to 307.0 m depth before being lost in alluvium. DDH-3A (drilled from a location adjacent to DDH-3) intersected bedrock at 312 m and cored until a depth of 430.8 m, retrieving 118.4 m of the core. Although boreholes had been drilled in this region during past exploration efforts looking for coal [38,39], these are presumed to be the first deep drill holes to intersect Precambrian bedrock in the Narmada Son lineament.

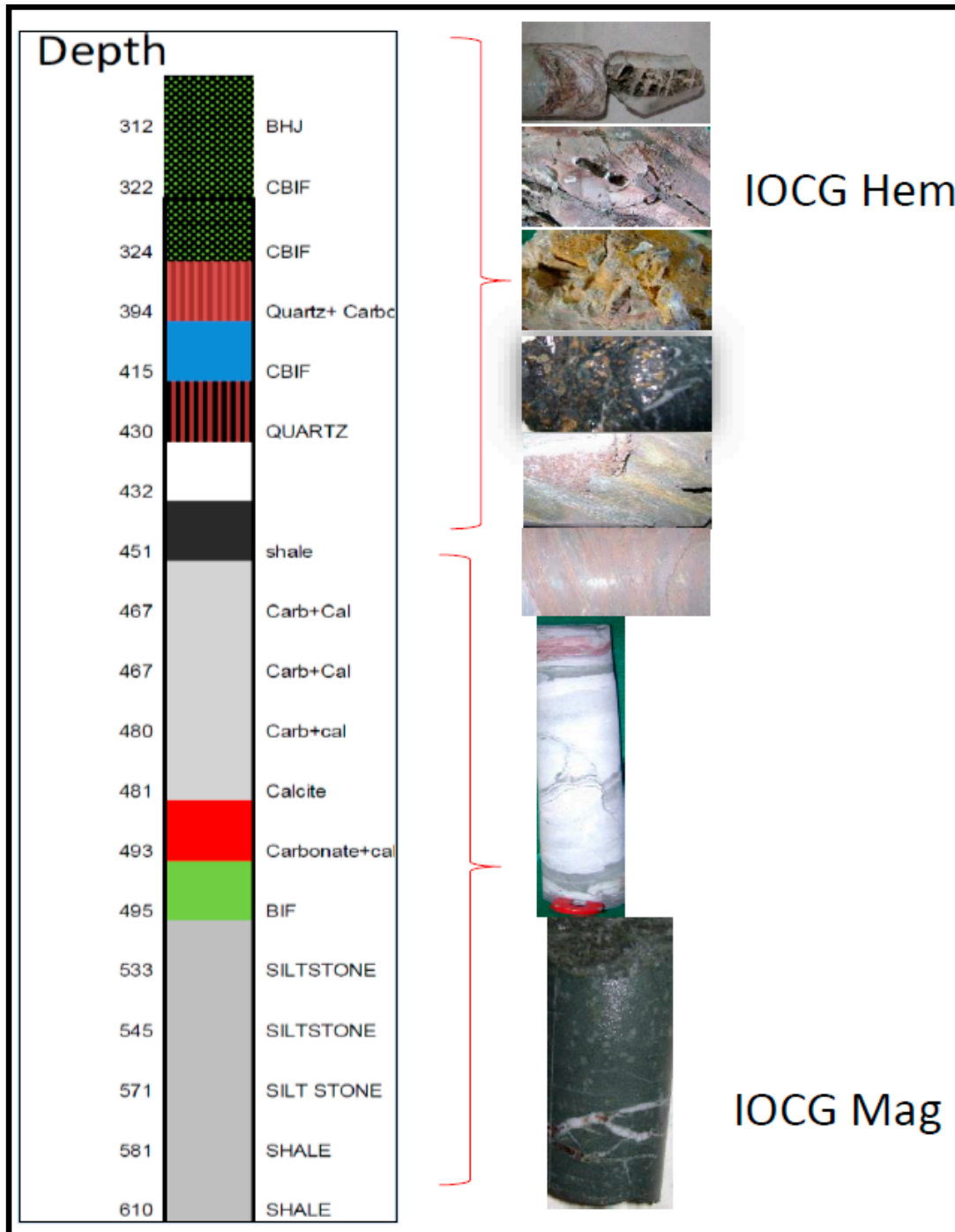


Figure 4. Core Log, Lithounits and core section of borehole DDH-1.

Table 2. Core section lithology of DDH-1.

Depth (in mts)	Litho-Unit	Description
312	BHJ	Dark brown to reddish brown in colour, intensely weathered and fractured, banded-hematite-jasper (BHJ), non-magnetic, specular hematite showing metallic lustre thin < 1 mm, fine grained jasper and hematite, soft yellow limonitic staining is noted at the fractured planes. The sulphides are pyrite, chalcopyrite and iron hydroxide like hematite.
322	Cherty IF	Weathered cherty iron bearing formation, the fine grained chert is hard and shiny lustre with sulphides and mostly pyrite, chalcopyrite and weathered staining on surface could be due leaching of iron oxides
324	Cherty IF	Weathered cherty iron bearing formation, the fine grained chert is hard and shiny lustre with sulphides and mostly pyrite, chalcopyrite and weathered staining on core surface.
394	Quartz + Carbonate	Dark brown to reddish brown in colour, intensely weathered and fractured, banded-hematite-jasper (BHJ), non-magnetic, specular hematite showing metallic lustre thin < 1 mm, fine grained. Due to intense weathering process the argillite's are altered to clay and to limonitic (yellow powdery nature) at carbonate show reactive nature with intense effervescence
415	CIF	Weathered cherty iron bearing formation, the fine grained chert is hard and shiny lustre with sulphides and mostly pyrite, chalcopyrite and weathered staining on surface could be due leaching of iron oxides.
430	Quartz	Fine grained quartz vein sample with saccharoidal texture.
450	Shale	Grey to dark grey in colour, very fine grained, carbonate rock with calcite occurring as grey bands of sulphidic minerals and often as relict textures. Both fine bands of purple coloured minerals varying from white to purple green.
467	Carbonate + Calcite	Carbonate show reactive nature with intense effervescence with typical calcite texture perfect cleavage and conchoidal with brittle around with gentle hardness.
480	Carbonate + Calcite	Carbonate show reactive nature with intense effervescence with typical calcite texture perfect cleavage and conchoidal with brittle around with gentle hardness.
481	Calcite	Calcite typical texture with perfect cleavage and conchoidal with brittle around with gentle hardness.
493	Carbonate + Calcite	Carbonate show reactive nature with intense effervescence with typical calcite texture perfect cleavage and conchoidal with brittle around with gentle hardness.
495	Iron Formation	Dark brown to reddish brown in colour, intensely weathered and fractured, banded-hematite-jasper(BHJ), non-magnetic, specular hematite showing metallic lustre thin < 1 mm, fine grained jasper and hematite, soft yellow limonitic staining is noted at the fractured planes. The sulphides are pyrite, chalcopyrite and iron hydroxide like hematite.
533	Siltstone	Grey to dark grey in colour, very fine grained, carbonate rock with calcite occurring as bands with grey mineral and often as relict texture, fine bands of purple coloured mineral (carbonate—as it reacts with HCl), the colour of carbonates vary from white to purple and green; fractured. Magnetite (very fine-grained) crystals as fine zones, Pyrite, Chalcopyrite.
545	Siltstone	Grey to dark grey in colour, very fine grained, carbonate rock hard and fissile. The colour of carbonates vary from white to purple and green; fractured. Magnetite (very fine-grained) crystals as fine zones, Pyrite, Chalcopyrite.
571	Siltstone	Grey to dark grey in colour, very fine grained, carbonate rock with calcite occurring as bands with grey mineral and often as relict texture, fine bands of purple coloured mineral (carbonate—as it reacts with HCl), the colour of carbonates vary from white to purple and green; fractured. Magnetite (very fine-grained) crystals as fine zones, Pyrite, Chalcopyrite.
581	Siltstone	Grey to dark grey in colour, very fine grained, carbonate rock with calcite fractured. Magnetite (very fine-grained) crystals as fine zones, Pyrite, Chalcopyrite and other sulphides.
610	Shale	Dark grey to black in colour, hard, very fine grained shale with inter-layers of carbonate; well foliated, fine grains sulphides (pyrite) randomly oriented.
610	Shale	Dark grey to black in colour, hard, very fine grained shale with inter-layers of carbonate; well foliated, fine grains sulphides (pyrite) randomly oriented.

The lithologies encountered in DDH3 consist of banded chert and fine-grained felsic tuff. Some of the beds are thinly laminated, and others are folded in convoluted patterns. Most notably, the drilling intersected an approximately 50 m thick Magnetite-bearing BIF assemblage. The samples contain banded hematite jaspelite (BHJ) and banded Magnetite (BM) iron formation. Locally, both foliaform and cross-cutting quartz veinlets, with and without traces of fine-grained pyrite are present. All samples have pervasive carbonate alteration. The BIF assemblage likely belongs to the Mahakoshal Supergroup of Archean to early Proterozoic age [30]. This Magnetic anomaly could be explained by the Magnetism method response from underlying Magnetite bearing "banded iron formation" or BIF with around 80% ferruginous chert-bearing Magnetite (BM), banded hematite jaspelite (BHJ) oxidized iron formations.

4.2. Magnetic Anomaly Modelling

The Magnetic anomalies interpretation is normally carried by Matching observed and calculated values of the anomalous Magnetic field. Talwani and Heirtzler (1964) were first to examine a nonmagnetic space containing a uniformly Magnetized two-dimensional structure approximated by a polygonal prism and to suggest a numerical and computational technique of the forward modeling [40].

The modelling is based on the measurements sampled at 200 m spacing for a 15 km long profile with traverse bearing of 170–350° (Figures 5 and 6). The observed ground TMI anomaly is bipolar in nature with an amplitude of ~1200 nT (Figure 6). The basement depth is estimated and calculated using a 1D log normalized radially averaged power spectrum [41,42] (Figure 7a,b). The straight line part of the spectrum at low wave number is considered for depth estimation, ~300 m is attributed to the core litho-log of DDH-1 borehole i.e., top alluvium, outer hematite, inner hematite, alteration of sodic/potassic rocks, hematite breccia, hematite breccia with quartz veinlets and at depth a Massive Magnetite. To understand the signatures of the Magnetic anomalies, initially a synthetic modeling is carried out. (Figure 8) As, the present study area is located in the south of Gadarwara, m.P, Central India bounded by geographic longitudes 78.7931° to 78.8173° and latitudes 22.7651° to 22.8743°. To estimate the geomagnetic components such as Total Magnetic field, Inclination and Declination, we adopted International Geomagnetic Reference Field (IGRF) model-2005 which is closest to surveyed year 2006. As per the IGRF-2005 model, the Total Magnetic Intensity field, geomagnetic inclination and declination of the study area are 44,900 nT, 33° and -0.43° respectively using Geosoft, 2006 version. The main objective of the synthetic model is to understand the shape of the Magnetic anomaly at this location with respect to observed field Magnetic anomaly. The shape of synthetic Magnetic anomaly will provide the origin of the Magnetic sources at the time of formation. In general, shape of the geomagnetic anomaly varies from equator to pole with a high negative anomaly peak at equator, bi-polar anomaly at 45° latitude and high positive anomaly peak at poles from south to north [43]. The nature of Magnetic anomaly at this geomagnetic latitude is also dependent to width, depth, depth extent, susceptibility of the Magnetic source, however these parameters influence the width and amplitude of the anomaly only. Hence synthetic anomaly is generated with the known constraints such as Magnetic total field, inclination and declination (IGRF, 2005 model), depth (from DDH 1 borehole data), width [31], dip [31] of the Magnetic sources. In the present case, we observed similarities both in synthetic and observed Magnetic i.e., high positive to low negative from south to north. Hence, remanence Magnetisation might be not present in the causative sources. The shape and width of the anomaly suggests a basement source up to 3.5 km in width and Rule of thumb depth estimations and examination of the amplitude fall-off rates suggest a depth to Magnetic source of approximately 396 m depth.

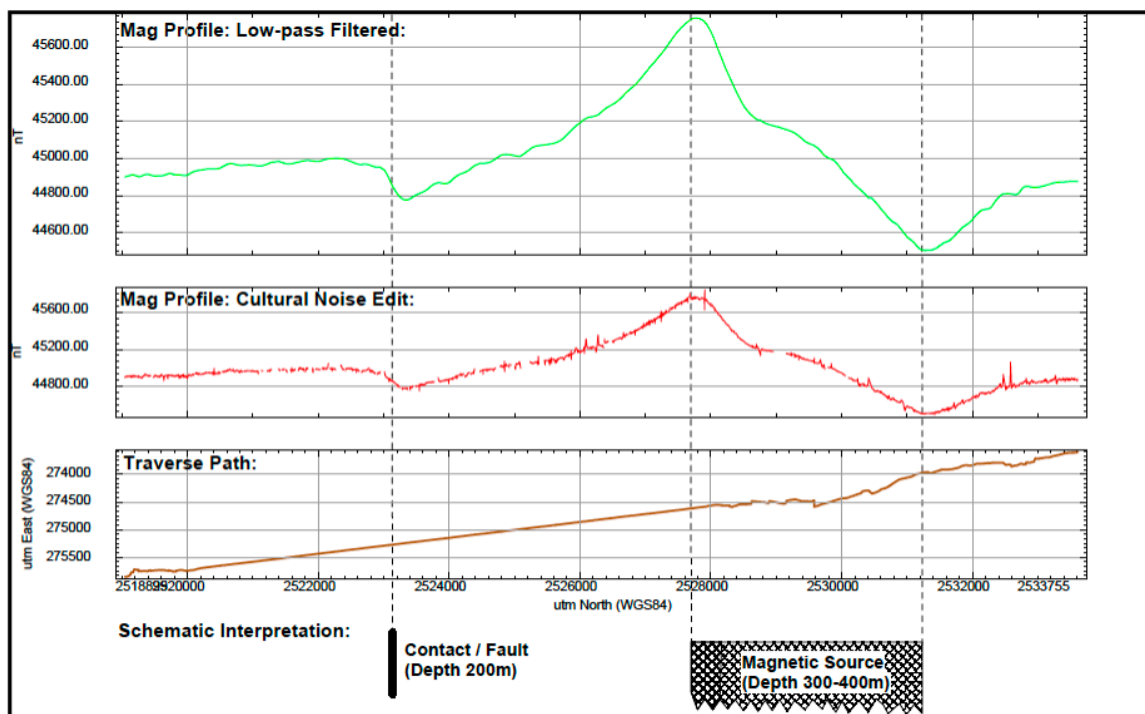


Figure 5. The Magnetic profile along traverse path, Magnetic data and low pass filter.

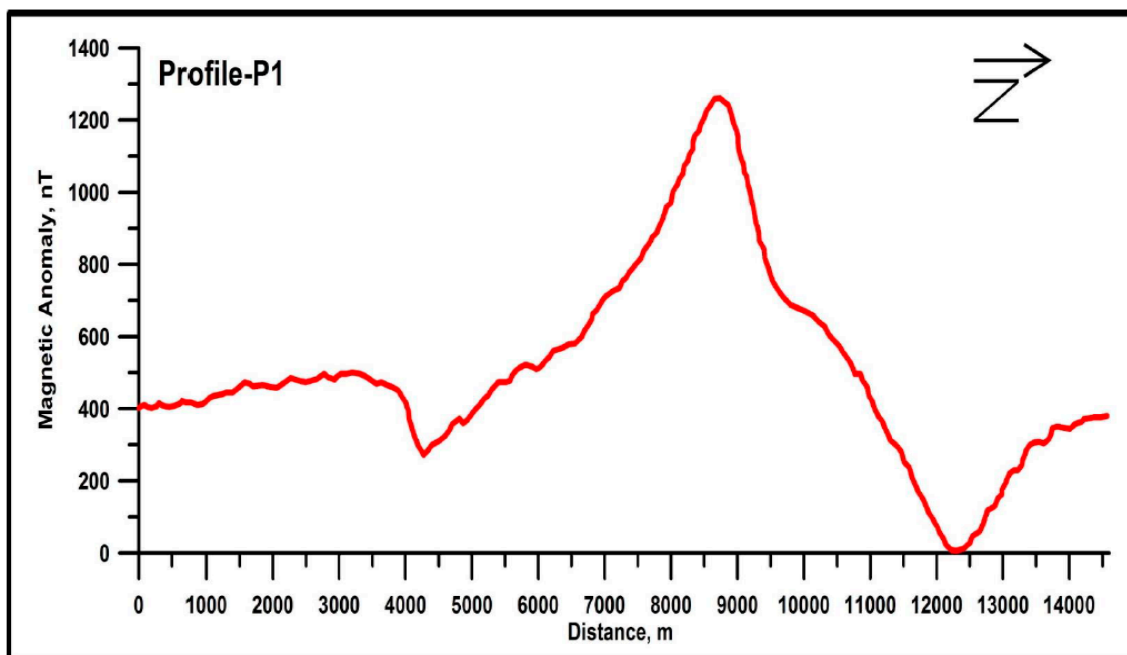


Figure 6. Observed total intensity Magnetic anomaly along profile P1.

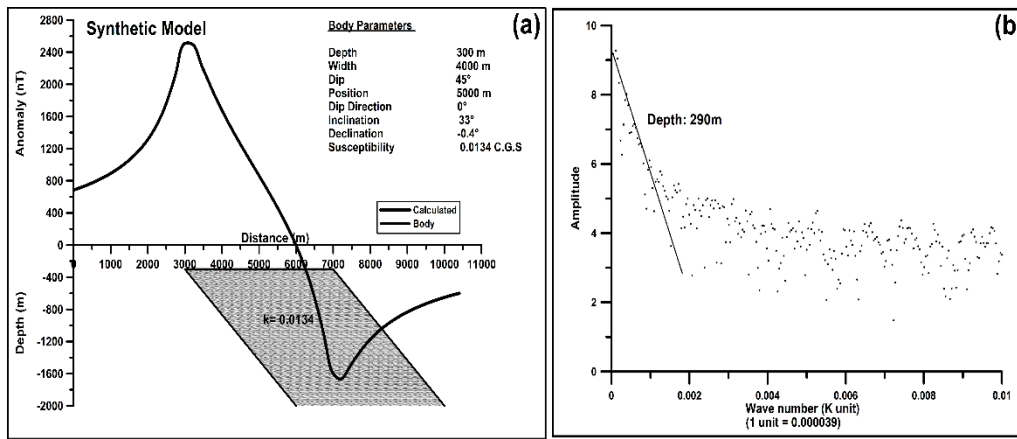


Figure 7. (a) synthetic Magnetic anomaly at geomagnetic latitude and (b) power spectrum Map showing the depth.

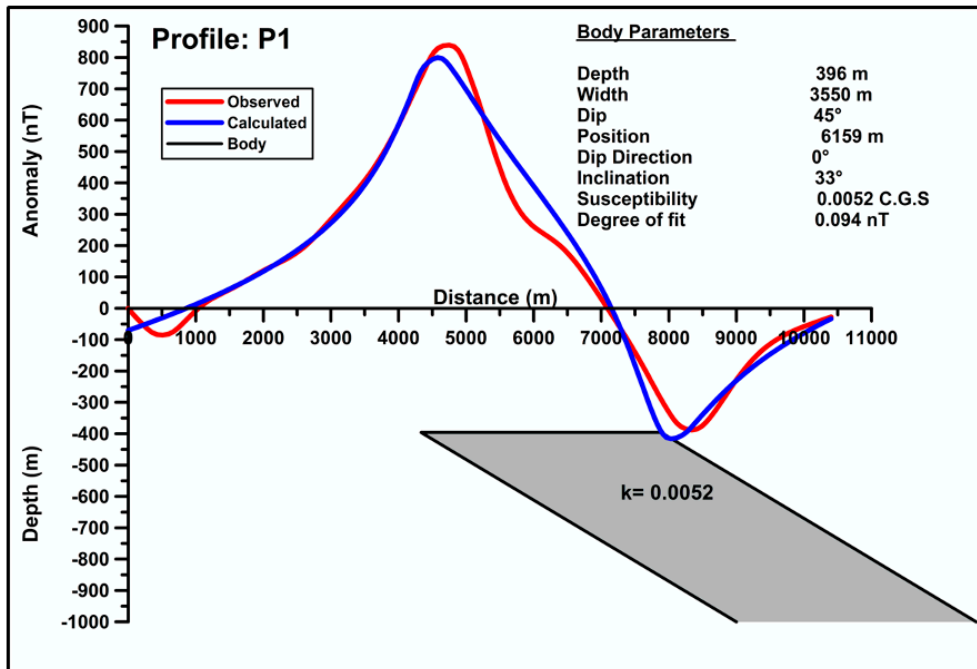


Figure 8. Interpreted 2D depth model for Magnetic anomaly.

The two dimensional model studies were carried using MaGMOD, Ltd., Toronto, Canada [31,44]. The geomagnetic Inclination and declination (33° and -0.4°), depth and width (300 m and 2000 m) of the causative source, dip (45°), Magnetization (600 nT) and strike (E-W) direction were used as initial inputs. A bipolar anomaly between 4000 and 14,500 m is considered for model studies from the profile P1 (Figure 8). The calculated Magnetic anomaly from the interpreted depth model corroborated with the observed anomaly with an R.M.S. error of 0.094 nT (Figure 8). The model studies suggest that the signature of high Magnetic anomaly is obtained from the surface to a depth of 400 m, with the mineralized body width of 3500 m at a dip angle of 45° towards north direction. The magnetic susceptibility 0.0052 C.G.S. units correspond to hematite with quartz veinlets lithology.

There is a slight possibility that an additional Magnetic source is located on the southern edge of the broader Magnetic source Manifested by a bipolar anomaly super-position on the Magnetic high coincident with the southern edge. An additional anomaly in the southern portion of the traverse is indicative of a contact or faulting. In general, the magnetic signatures of IOCG systems reflect superposed or juxtaposed Magnetic anomalies inferring a deeper source for the Magnetic anomaly.

The possible reason could be that the hematite rich zone has been heated >600 °C by regional or contact metamorphism and therefore might have acquired sufficient remanence to produce Magnetic anomalies. Hence, the observed Magnetic anomaly is due to the presence of hematite or Magnetite, weathered and oxidised/brecciated iron rich layers at 396 m depth.

5. Discussion

The drill holes DDH 1 and DDH 3 are the first deep drill holes to intersect Precambrian bedrock in the Narmada Son lineament. Unusual geological litho-units cause the geophysical anomaly at depths probably due to underlying Magnetite bearing "banded iron formation" or BIF of around 80% ferruginous chert-bearing Magnetite (BM), banded hematite jaspelite (BHJ) oxidised iron formations. The basinal fluids preserved in evaporate-bearing sedimentary successions are the important and significant contribution to the fluid budget of hematite-rich IOCG systems. The mineral footprints in the core samples investigated from Gadarwara suggest that samples have undergone hydrothermal, and oxidation alterations of primary mineralisation [45]. The hydrothermal footprint is expressed by intense silicification related to pervasive quartz veinlets. These hydrothermal alteration systems [2,46,47] are typically expressed by silicate and oxide alteration minerals and can be characterized by three zones including: (1) An upper hematite- and/or Magnetite-rich zone, ~1–3 km in horizontal diameter, associated with copper and iron sulphides (e.g., chalcopyrite, bornite and pyrite) together with sericite, chlorite and carbonate alteration. In the Olympic Dam copper-gold province it is evident that higher grade copper-gold and/or uranium/rare earth element mineralisation occurs within the upper, hematitic zones [48]. (2) A mid-depth zone rich in Magnetite with biotite or potassium feldspar \pm minor pyrite, showing petrological similarities to core samples investigated typically of a few hundred meters to ~1–3 km in lateral dimensions. (3) A lower zone with sodic-calcic alteration rich in albite, actinolite \pm clinopyroxene (e.g., diopside), with minor Magnetite, potentially extending laterally up to 5–10 km in Major IOGC provinces such as the Olympic copper-gold province and Cloncurry IOGC district. The major four essential components in IOCG ore systems of Olympic Dam type are (a) the crustal architecture i.e., reactivated orogenic architecture occurring at craton Margin settings, (b) The energy sources to ascent the hydrothermal fluids i.e., High temperature associated with A and I types felsic and coeval Mafic-ultramafic Magmatism. The two stage of mineralization from deep source high temperature brine of Magmatic-hydrothermal and/or basinal origins and shallow sourced lower temperature fluids of meteoric origin, (c) early high temperature iron oxides and (d) late Cu-Au, Cu from Mainly Mafic sources and U could be from felsic sources and large scale potassic alteration features. The extensive alteration zones of Magnetite, K-Feldspar, actinolite, pyrite, apatite, carbonate, quartz and chalcopyrite produce the Magnetic anomalies [7]. The similarities of oxidised alteration zones May be present above or lateral to Magnetite alteration with high grades of Cu-Au mineralisation predicted within hematitic alteration near the transition to Magnetite. Whereas, in Cloncurry Cu-Au mineralization overprinting the banded iron formation in similarity to Gadarwara type.

On a cratonic scale in all the IOCG districts the lithounits include felsic intrusions, Mafic dykes, Mafic intrusions, felsic volcanic, BIFs, clastic sediments and carbonate meta evaporates. The Gadarwara is located at the craton Margin hosting meta-sediments especially BIFs with high Magnetite contents with cross cutting dykes, especially associated with shales. The association of copper-gold mineralization with hematitic alteration and hydrothermal Magnetite with associated Cu-Au transported by late oxidizing brine solutions that had reacted with meta-sedimentary rocks such as BIFs. The shales could have supplied required sulphur for the sulphide enrichments especially copper sulphides such as chalcopyrite. The geological exploration indicators of REE-bearing meta sedimentary hosts include intraplate continental environments rifting and/faulting, alteration halos, and indicator minerals.

The key styles of copper-gold mineralisation in the Cloncurry district, to the east of Mount Isa is associated with Magnetite and potassium feldspar alteration (e.g., Ernest Henry deposit) whereas another style occurs with pyrrhotite and Magnetite (e.g., Eloise deposit. Both the Ernest Henry and

Eloise deposits are closely associated with intense Magnetite alteration. In several, Australian deposits Pressure-Temperature modelling shows that the contact zones between Magnetite- and hematite-rich alteration is highly favourable for the formation of higher grade copper-gold mineralisation [5] similar to Gadarwara (Figures 9 and 10). Such redox gradients also appear to be important in the high grade gold-copper-bismuth deposits of the Tennant Creek district, where both Magnetite- and hematite-rich deposits are present in association with chlorite \pm sericite alteration [6–9]. Therefore, the most attractive copper-gold exploration targets identified in Olympic Dam, Tennant creek [4,7], are those relatively small bodies (e.g., <15 km width) where exceptionally dense and Magnetic Material (magnetite \pm pyrrhotite) is laterally or vertically in contact with exceptionally dense bodies of low Magnetic susceptibility (e.g., hematite \pm pyrite \pm copper sulphides). At Olympic Dam, the zonation is vertically from Magnetite dominated at depth to hematite on surface i.e., upper levels. This pattern could have been altered by Major tectonic activity in the form of tilting or by faulting. It leads to debate on the Magnetic signatures of IOCG deposits which May reflect superposed or juxtaposed Magnetic anomalies [8,49]. At Gadarwara the litho-units like iron rich laminated mudstone-siltstone at depth probably formed as a submarine sedimentary facies. The retrogression and or hydrothermal alteration at upper greenschist/lower amphibolite facies led to Magnetite replacement of protolithic hematite. At lower temperature <150 °C veins of hematite develop chalcedony of quartz [1,2]. In Table 3, the comparison of IOCG deposits like Olympic Dam, Cloncurry, Kiruna, Phalborwa and Bayan Obo show similarities in ore body shape such as 1. irregular breccia, mineralization style 2. dominant minerals like Magnetite, hematite and copper sulphides and 3. enriched in copper, gold, iron ore, and REE enrichments. 4. The alteration zonation is ranging from sodic to calcic and potassic corroborated in drill core samples with Gadarwara.

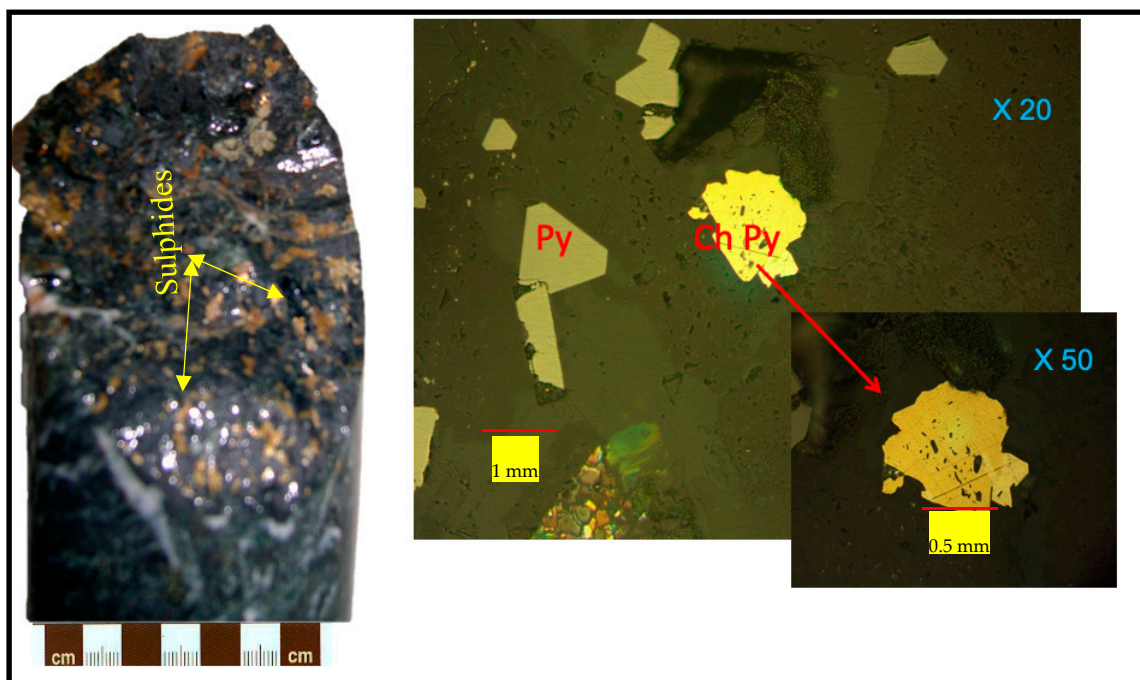


Figure 9. The drill core with sulphides, and petrography reveals Pyrite (Py) and Chalcopyrite (Chpy).

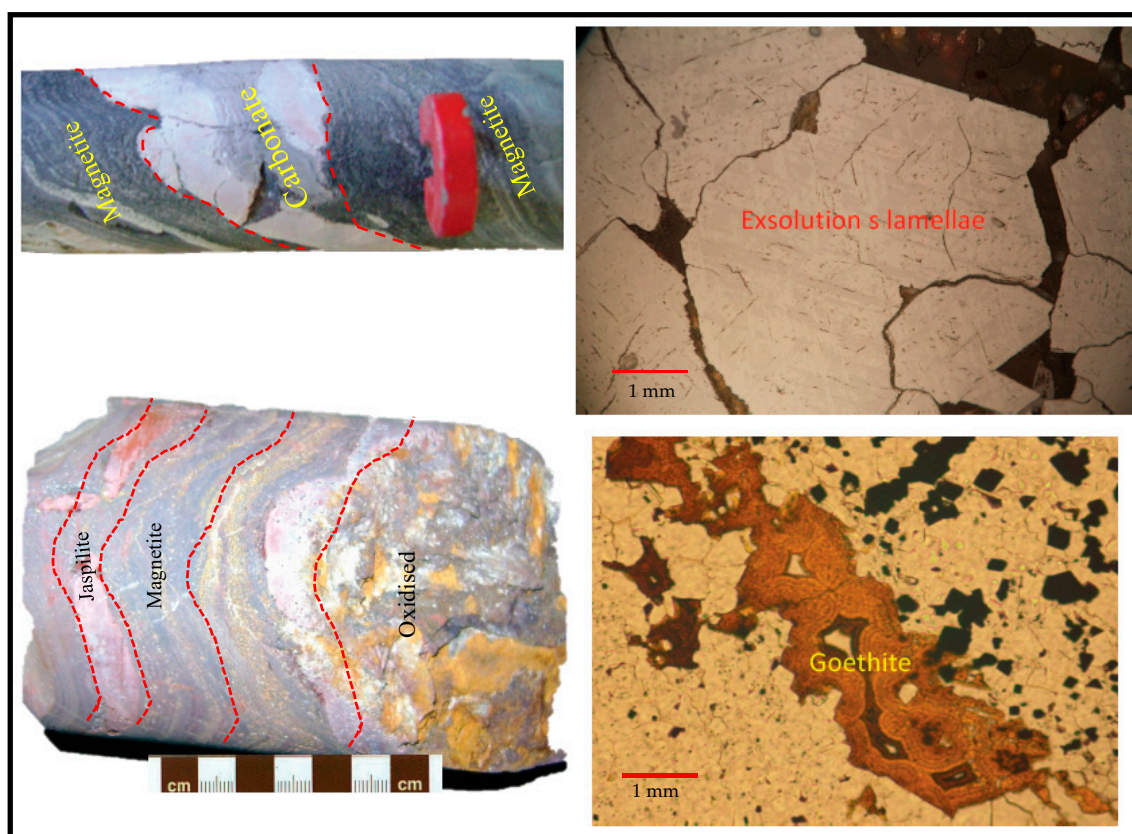


Figure 10. Oxidized brecciated iron formation with goethite and martite.

Table 3. Comparison of similarities of Gadawara with other IOCG deposits.

Giant Ore Deposit	Type	Mineralisation	Alteration	Commodity	Orebody
Olympic Dam, Australia	Olympic Dam	Magnetite-hematite-bornite-chalcopyrite-breccia Matrix	Potassic	Fe, Cu, Au, Ag, REE, U	Pipe like and irregular breccia
Osborne, Queensland, Australia	Cloncurry	Magnetite-hematite-apatite replaced by Cu-Fe sulphides, Au etc.	Potassic	Cu, Au, Ag, Bi, Co, W	Stratabound vein, breccia
Kiirunavaara, Sweden	Kiruna	Massive Magnetite-apatite-actinolite	sodic	Fe ± Cu, Au	Tabular, pipe like, irregular
Magnitogorsk, Urals, Russia	Iron skarn	Massive Magnetite-garnet-pyroxene	Sodic	Fe ± Cu, Au	Stratabound lensoid, irregular
Phalaborwa, South Africa	Phalaborwa	Magnetite, apatite, fluorite.Cu sulphides	Sodic + potassic	Cu, Au, Ag, REE, PGE, vermiculite, Magnetite, P, U, Zr, Se, Te, Bi	Veins, layers, disseminations
Bayan Obo, Mongolia, China	Bayan Obo	Magnetite, hematite, bastnaesite, Fe-Ti-Cr-Nb oxides, monazite	Weathering of Fe oxides	REE	disseminations
Madhya Pradesh, Central India	Gadarwara	Magnetite, hematite, Cu-Fe, Au, monazite, apatite, zircon, sulphides	Sodic + potassic	Cu, Ni, Au, REE	Irregular breccia
Western Bastar Craton, India	Thaneswasna	Magnetite, hematite, pyrite, arsenopyrite, chalcopyrite, monazite	Potassic	Fe-Cu-Ba-Au-Ag-Th	breccia

The interpretation of airborne and ground Magnetic profiles using a full dike model provided the initial clues with respect to depth, width, dip, and susceptibility of the causative source as 200 m, 4000 m, 42° N, and 0.004 CGS, respectively, in the Gadawara region [2]. In the initial stages of exploration this paved a way for further detailed ground survey and drilling data were corroborated with the 2D Magnetic modelling studies. The drill hole DDH-1 assay log (Figure 11) distinctly show enrichment of Cu, Au, Cr, U and Σ REE's (total REE's) and corroborated with global model (Figure 12) as Gadawara type (GT).

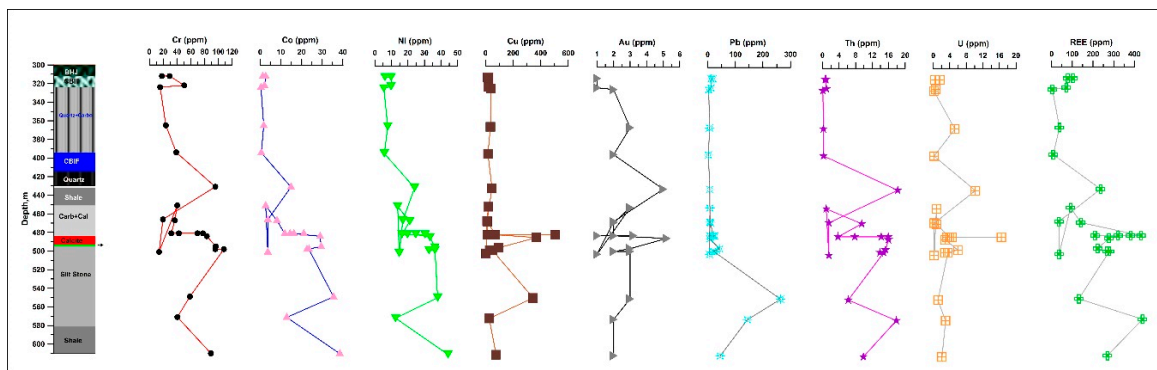


Figure 11. Lithology of DDH-1 drill core with vs assay data.

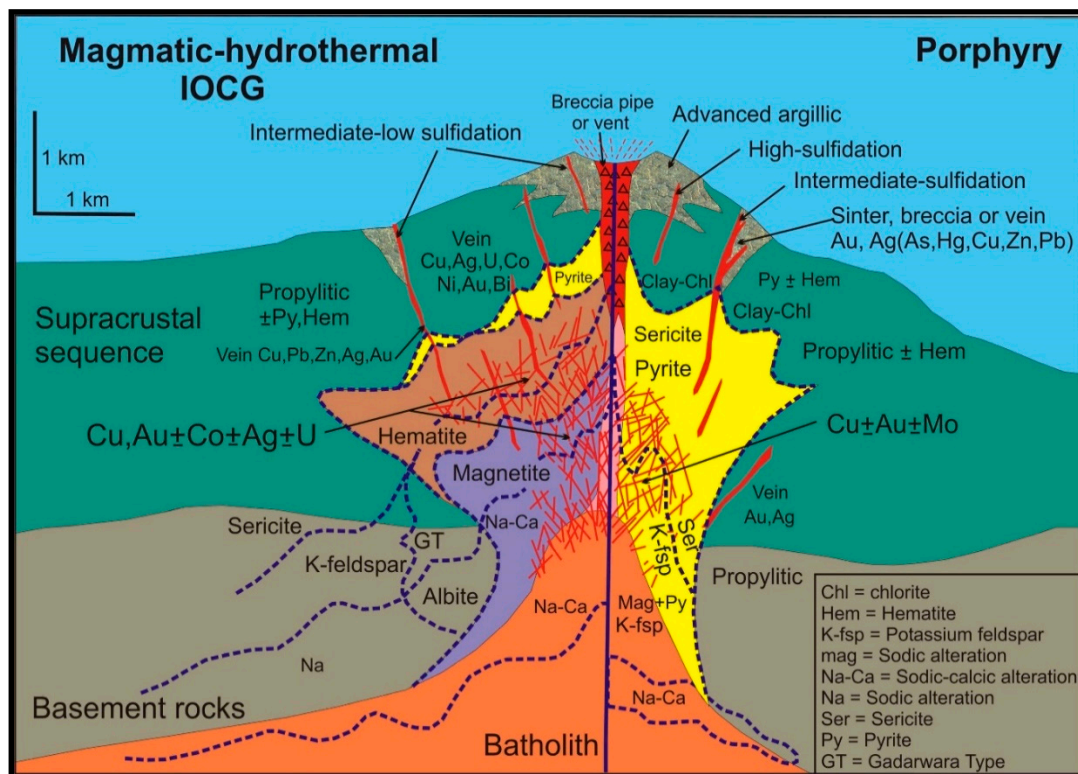


Figure 12. Modified Schematic model for Magmatic-hydrothermal systems illustrating relationship between S-rich porphyry Cu ± Mo ± Au deposits (right side) and S-poor Magmatic-hydrothermal iron oxide-copper-gold (MH-IOCG) deposits (left side). Approximate hydrothermal mineral transitions and relative spatial footprint are shown for albite–K-feldspar, K-feldspar–sericite, and magnetite–hematite transitions. Prograde and retrograde overprinting of alteration assemblages and mineralization is common. Spatial relationships for porphyry deposits after Seedorff et al. (2005) [50], Sillitoe (2010) [51], and Richards (2011) [52]; for MH-IOCG, after Hitzman et al. (1992) [48], Williams et al. (2005) [49], and Mumin et al. (2010) [53]. (Figure modified under “Fair- Use” permission from GSA) source: Magmatic-hydrothermal processes within an evolving Earth: Iron oxide-copper-gold and porphyry Cu ± Mo ± Au deposits *Geology* [54].

6. Conclusions

Combining our interpretations and drill core observation, we demonstrated the presence of favourable IOCG with Au-Cu mineralization, which are spatially correlated with the redox boundary. The anomaly has been confirmed by integrating the geophysical and geochemical investigations. The 2D Magnetic model suggests a depth of 396 m with a width of 3.5 km, with a north dipping body

and southwards bipolar anomaly also suggesting a fault. Structural control like a fault also suggest a significant scope for further investigations. The main key variables giving rise to Gadaruwara IOCG are the local host rock types which are diverse in nature. Variation in depth in different structural settings such as breccia at shallow levels and shear hosted at deeper levels. The alteration such as hematite at shallower levels and Magnetite at deeper levels identified at 396 mts in drill hole. Basinal fluids preserved in evaporate-bearing sedimentary successions are important and significant contribution to fluid budget of hematite-rich IOCG system. The mineral footprints in the core samples investigated from Gadaruwara suggest that samples have undergone hydrothermal, and oxidation alterations of primary mineralisation. The Potential indicator minerals comprise sheet silicates (i.e., kaolinite, montmorillonite, dickite, mica, chlorite), iron oxides, quartz and carbonates. The PT-variations May have caused a regional transformation of kaolin group minerals and smectites to mica and chlorite. The hydrothermal footprint is expressed by intense silicification related to pervasive quartz veinlets. The oxidation of primary sulphides and iron oxides, such as hematite, Magnetite, iron carbonates (e.g., ankerite, siderite etc.) is typical of but not exclusive to IOCG type of mineralisation. The BIFS are highly oxidised with intense brecciation with hydrothermal overprinting. The EPMA analyses reflect abundant low Ti-Fe oxides, Magnetite, hematite with grunerite and Fe-bearing actinolite. There is also Na-K intense metasomatism and Gadaruwara is present in a rift type of tectonic environment

Author Contributions: Data curation, P.V.S.R.; formal analysis, K.S.K.; methodology, P.V.S.R. and K.S.K.; project administration, P.V.S.R. and K.S.K.; resources, P.V.S.R.; writing—original draft, P.V.S.R.; writing—review and editing, P.V.S.R. and K.S.K. All authors have read and agreed to the published version of the manuscript.

Funding: The research has no external funding

Acknowledgments: P.V.S.R. thank C. Hart for hosting him as a visiting scientist, at MDRU, UBC, Canada. We thank Andrew Nevin, CMD of Adi Gold Mining Pvt Ltd., and M. K. Sen for his support during the study, CSIR, New Delhi, for providing RRF and V.M. Tiwari, Director, CSIR-NGRI for his support. Benjamin, CSIR-TWAS fellow and Hari for preparing figures. We thank three anonymous reviewers for their excellent reviewing which helped to improve the quality of Manuscript. P.G. Eriksson for his comments and valuable discussions during Manuscript preparation. R.K.W. Merkle for his comments and thoughtful debate on initial MS.

Conflicts of Interest: The authors declare no conflict of interest.

References

1. Hitzman, M.W.; Porter, T.M. Iron oxide-Cu-Au deposits: What, where, when, and why. *Hydrothermal Iron Oxide Copp. -Gold Relat. Depos. A Glob. Perspect.* **2000**, *1*, 9–25.
2. Hitzman, M.W.; Porter, T.M. Current Understanding of Iron Oxide Associated-Alkali Altered Mineralised Systems: Part II, A Review. In *2010 Hydrothermal Iron Oxide Copper-Gold and Related Deposits: A Global Perspective*; Porter, T.M., Ed.; PGC Publishing: Adelaide, Australia, 2010; Volume 3, pp. 33–106.
3. Bastrakov, E.N.; Skirrow, R.G. Fluid evolution and origin of Cu and Au prospect in the Olympic dam district, Gawler Craton, South Australia. *Econ. Geol.* **2007**, *102*, 1415–1440. [[CrossRef](#)]
4. Skirrow, R.G.; Bastrakov, E.N.; Barovich, K.; Fraser, G.L.; Creaser, R.A.; Fanning, C.M.; Davidson, G.J. Timing of iron oxide Cu-Au-(U) hydrothermal activity and Nd isotope constraints on metal sources in the Gawler craton, South Australia. *Econ. Geol.* **2007**, *102*, 1441–1470. [[CrossRef](#)]
5. Ehrig, K.; McPhie, J.; Kamenetsky, V.S. Geology and Mineralogical Zonation of the Olympic Dam Iron-Oxide-Cu-U-Au-Ag Deposit, South Australia. Available online: https://www.researchgate.net/profile/Vadim_Kamenetsky/publication/291217932_Geology_and_mineralogical_zonation_of_the_Olympic_Dam_iron_oxide_Cu-U-Au-Ag_deposit_South_Australia/links/5c403ec1a6fdccd6b5b2dd26/Geology-and-mineralogical-zonation-of-the-Olympic-Dam-iron-oxide-Cu-U-Au-Ag-deposit-South-Australia.pdf (accessed on 6 July 2020).
6. Groves, D.I.; Bierlein, F.P.; Meinert, L.D.; Hitzman, M.W. Iron oxide copper-gold (IOCG) deposits through Earth history: Implications for origin, lithospheric setting, and distinction from other epigenetic iron oxide deposits. *Econ. Geol.* **2010**, *105*, 641–654. [[CrossRef](#)]

7. Skirrow, R.G. Gold-copper-bismuth deposits of the Tennant Creek district, Australia: A reappraisal of diverse high-grade systems. In *Hydrothermal Iron Oxide Copper-Gold & Related Deposits: A Global Perspective*; Porter, T.M., Ed.; PGC Publishing: Adelaide, Australia, 2000; Volume 1, pp. 149–160.
8. Williams, P.J.; Corriveau, L.; Mumin, A.H. Magnetite-group IOCGs with special reference to Cloncurry (NW Queensland) and northern Sweden: Settings, alteration, deposit characteristics, fluid sources, and their relationship to apatite-rich iron ores. *Geol. Assoc. Can. Short Course Notes* **2010**, *20*, 23–38.
9. Corriveau, L.; Montreuil, J.-F.; Potter, E.G. Alteration facies linkages among IOCG, IOA, and affiliated deposits in the Great Bear Magmatic zone. *Can. Econ. Geol.* **2016**, *111*, 2045–2072. [[CrossRef](#)]
10. Torresi, I.; Xavier, R.P.; Bortholoto, D.F.; Monteiro, L.V. Hydrothermal alteration, fluid inclusions and stable isotope systematics of the Alvo 118 iron oxide–copper–gold deposit, Carajás Mineral Province (Brazil): implications for ore genesis. *Miner. Depos.* **2012**, *47*, 299–323. [[CrossRef](#)]
11. Hunt, J.A.; Baker, T.; Thorkelson, D.J. A review of iron oxide copper-gold deposits, with focus on the Wernecke Breccias, Yukon, Canada, as an example of a non-magmatic end member and implications for IOCG genesis and classification. *Explor. Min. Geol.* **2007**, *16*, 209–232. [[CrossRef](#)]
12. Mumin, A.H. The IOCG-Porphyry-Epithermal Continuum of Deposit Types in the Great Bear Magmatic Zone, Northwest Territories, Canada. In *Exploring for Iron Oxide Copper-Gold Deposits: Canada and Global Analogues*; Corriveau, L., Mumin, H., Eds.; Geological Association of Canada: St. John's, NL, Canada, 2010; pp. 59–78.
13. Knight, J. The Khetri copper belt, Rajasthan: iron-oxide copper-gold terrane in the Proterozoic of NW India. In *Hydrothermal Iron Oxide Copper-Gold & Related Deposits: A Global Perspective*; Porter, T.M., Ed.; PGC Publishing: Adelaide, Australia, 2002; Volume 2, pp. 321–341.
14. Pal, D.C.; Barton, M.D.; Sarangi, A.K. Deciphering a multistage history affecting U-Cu (-Fe) mineralization in the Singhbhum Shear Zone, eastern India, using pyrite textures and compositions in the Turamdih U-Cu (-Fe) deposit. *Miner. Depos.* **2009**, *44*, 61–80. [[CrossRef](#)]
15. Corriveau, L.; Potter, E.G.; Montreuil, J.F.; Blein, E.K.; Fabris, A.; Reid, A.J. Alteration facies of IOA, IOCG and affiliated deposit: Understanding the similarities recognising the diversity of the ore systems GSA. In Proceedings of the GSSA Workshop, Québec, QC, Canada, 11–12 May 2019.
16. Corriveau, L.; Williams, P.J.; Mumin, A.H. Alteration vectors to IOCG mineralisation—From uncharted terranes to deposits. *Can. Glob. Analog.* **2010**, *20*, 89110.
17. Kirmani, I.R.; Chander, S. Petrology, geochemistry and fluid inclusion studies of Cu-Au mineralization in paleoproterozoic Salumber-Ghatol belt, Aravalli Supergroup, Rajasthan. *J. Geol. Soc. India.* **2012**, *80*, 5–38.
18. Dora, M.L.; Saha, A.K.; Randive, K.R.; Rao, K.K. Iron oxide–copper–gold mineralization at Thanewasna, western Bastar Craton. *Curr.Sci.* **2017**, *112*, 1045–1050. [[CrossRef](#)]
19. Shukla, A.K.; Behera, P.; Basavaraja, K.; Mohanty, M. Iron oxide–copper–gold-type mineralization in Machanur area, Eastern Dharwar Craton, India. *Curr. Sci.* **2016**, *5*, 1853–1858. [[CrossRef](#)]
20. NGRI. *High-Resolution Air Borne Geophysical Surveys for Mineral Exploration—Aeromagnetic Discovery of Gadarwara Gold Prospect*; NGRI Report; NGRI: Hyderabad, India, 2007; p. 59.
21. Mazumder, R.; De, S.; Sunder Raju, P.V. Archean-Proterozoic transition: the Indian perspective. *Earth Sci. Rev.* **2019**, *188*, 427–440. [[CrossRef](#)]
22. Crumansonata. Crumansonata Geoscientific studies of the Son–Narmada–Tapti Lineament Zone. *Geol. Surv. India Spec. Publ.* **1995**, *10*, 244.
23. Chakraborty, C.; Bhattacharya, A.A. The Vindhyan Basin: An overview in the light of crustal perspective. *Mem. Geol. Soc. India.* **1996**, *36*, 301–312.
24. Yedekar, D.B. The central Indian collision suture. *Geol. Surv. India, Spec. Publ.* **1990**, *28*, 1–4.
25. Acharyya, S.K.; Roy, A. Tectonothermal history of the Central Indian Tectonic Zone and reactivation of Major faults/shear zones. *J. Geol. Soc. India* **2000**, *55*, 239–256.
26. Chattopadhyay, A.; Khasdeo, L. Structural evolution of Gavilgarh-Tan Shear Zone, central India: A possible case of partitioned transpression during Mesoproterozoic oblique collision within Central Indian Tectonic Zone. *Precam. Res.* **2011**, *186*, 70–88. [[CrossRef](#)]
27. Raju, P.V.S.; Hart, C.; Kathal, P. Newly recognized IOCG-like mineralization at Gadarwara, m.P, India. *Mineral. Mag.* **2014**, *77*, 2026.

28. Mallet, F.R. On the Vindhyan Series, as exhibited in the north-western and central provinces of India. *Mem. Geol. Surv. India*. **1869**, *7*, 1–129.
29. Ghosh, D.B. The nature of Narmada-Son Lineament. *Geol. Surv. India Misc. Pub.* **1976**, *34*, 119–132.
30. Nair, K.K.K. Stratigraphy, structure and geochemistry of the Mahakoshal greenstone. *Mem. Geol. Soc. India*. **1995**, *37*, 403–432.
31. Babu, H.R. Relationship of gravity, Magnetic, and self-potential anomalies and their application to mineral exploration. *Geophysics* **2003**, *68*, 181–184. [[CrossRef](#)]
32. Bickford, M.E.; Mishra, M.; Mueller, P.A.; Kamenov, G.D.; Schieber, J.; Basu, A. U-Pb age and Hf isotopic compositions of Magmatic zircons from a rhyolite flow in the Porcellanite Formation in the Vindhyan Supergroup, Son Valley (India): implications for its tectonic significance. *J. Geol.* **2017**, *125*, 367–379. [[CrossRef](#)]
33. Ray, J.S.; Martin, M.W.; Veizer, J.; Bowring, S.A. U-Pb zircon dating and Sr isotope systematics of the Vindhyan Supergroup, India. *Geology* **2002**, *30*, 131–134. [[CrossRef](#)]
34. Kumar, S.; Schidlowski, M.; Joachimski, M.M. Carbon isotope stratigraphy of the Palaeo-Neoproterozoic Vindhyan Supergroup, central India: implications for basin evolution and intrabasinal correlation. *J. Palaeontol. Soc. India* **2005**, *50*, 65–81.
35. Jain, S.C.; Nair, K.K.K.; Yedekar, D.B. Tectonic evolution of the Son-Narmada-Tapti lineament zone. *Geol. Surv. India Spec. Pub.* **1995**, *10*, 333–371.
36. Mishra, D.C. *Gravity and Magnetic Methods for Geological Studies*; BS Publications: Hyderabad, India, 2011.
37. Rao, D.A.; Babu, H.R.; Sinha, G.S. Crustal structure associated with Gondwana graben across the Narmada-Son lineament in India: inference from aeromagnetism. *Tectonophysics* **1992**, *212*, 163–172. [[CrossRef](#)]
38. Medicott, H.B. Notes on Satpura Coal Basin. *Mem. Geol. Surv. India* **1873**, *10*, 133–188.
39. Medicott, H.B.; Blanford, W.T. *A Manual Geology of India*; Govt of India Press: Calcutta, India, 1879.
40. Talwani, M. Computation of Magnetic anomalies caused by two-dimensional bodies of arbitrary shape. *Comput. Miner. Ind.* **1964**, *1*, 464–480.
41. Spector, A.; Bhattacharyya, B.K. Energy density spectrum and autocorrelation function of anomalies due to simple Magnetic models. *Geophys. Prospect.* **1966**, *14*, 242–272. [[CrossRef](#)]
42. Spector, A.; Grant, F.S. Statistical models for interpreting aeromagnetic data. *Geophysics* **1970**, *35*, 293–302. [[CrossRef](#)]
43. MacLeod, I.N.; Jones, K.; Dai, T.F. 3-D analytic signal in the interpretation of total Magnetic field data at low Magnetic latitudes. *Explor. Geophys.* **1993**, *24*, 679–688. [[CrossRef](#)]
44. PGW. *Program Documentation-MAGMOD Version 1.4 Magnetic Interpretation Software Library*; Paterson, Grant and Watson Ltd.: Toronto, ON, Canada, 1982; p. 17.
45. Raju, P.V.S.; Hart, C.; Kathal, P. Integrated SWIR spectral and XRD studies on core samples from Gadarwara, Central India Craton, Madhya Pradesh, India-footprints for IOCG mineralisation. In Proceedings of the 14th SGA Biennial Meeting, Québec, QC, Canada, 20–23 August 2017; pp. 963–966.
46. Haynes, D.W.; Porter, T.M. Iron oxide copper (-gold) deposits: Their position in the ore deposit spectrum and modes of origin. *Hydrothermal Iron Oxide Copp. -Gold Relat. Depos. A Glob. Perspect.* **2000**, *1*, 71–90.
47. Hitzman, M.W.; Oreskes, N.; Einaudi, M.T. Geological characteristics and tectonic setting of proterozoic iron oxide (Cu-U-Au-REE) deposits. *Precambrian Res.* **1992**, *58*, 241–287. [[CrossRef](#)]
48. Belperio, A.; Flint, R.; Freeman, H. Prominent hill: a hematite-dominated iron oxide copper gold system. *Econ. Geol.* **2007**, *102*, 1499–1510. [[CrossRef](#)]
49. Williams, P.J.; Barton, M.D.; Johnson, D.A.; Fontboté, L.; De Haller, A.; Mark, G.; Marschik, R. Iron oxide copper-gold deposits: Geology, space-time distribution, and possible modes of origin. *Econ. Geol.* **2005**, *100*, 371–405. [[CrossRef](#)]
50. Seedorff, E.; Dilles, J.H.; Proffett, J.M., Jr.; Einaudi, M.T.; Zurcher, L.; Stavast, W.J.A.; Johnson, D.A.; Barton, M.D. Porphyry Deposits: Characteristics and Origin of Hypogene Features. *Econ. Geol.* **2005**, *100*, 251–298.
51. Sillitoe, R.H. Porphyry copper systems. *Econ. Geol.* **2010**, *105*, 3–41. [[CrossRef](#)]
52. Richards, J.P. Magmatic to hydrothermal metal fluxes in convergent and collided Margins. *Ore Geol Rev.* **2011**, *40*, 1–26. [[CrossRef](#)]

53. Mumin, A.H.; Phillips, A.; Katsuragi, C.J.; Mumin, A.; Ivanov, G. *Geotectonic Interpretation of the Echo Bay Stratovolcano Complex, Northern Great Bear Magmatic Zone*; Northwest Territories Geoscience Office: Yellowknife, NT, Canada, 2013; p. 35.
54. Richards, J.P.; Mumin, A.H. Magmatic-hydrothermal processes within an evolving Earth: Iron oxide-copper-gold and porphyry Cu ± Mo ± Au deposits. *Geology* **2013**, *41*, 767–770. [[CrossRef](#)]



© 2020 by the authors. Licensee MDPI, Basel, Switzerland. This article is an open access article distributed under the terms and conditions of the Creative Commons Attribution (CC BY) license (<http://creativecommons.org/licenses/by/4.0/>).